Dibromocarbene Functionalization of Boron Nitride Nanosheets: Towards Band-Gap Manipulation and Nanocomposite Applications

Toby Sainsbury[1,*], Arlene O'Neill[2], Melissa K. Passarelli[1], Maud Seraffon[1], Dipak Gohil[1], Sam Gnaniah[1], Steve J. Spencer[1], Alasdair Rae[1], Jonathan N. Coleman[2]

[1]*Materials Division, National Physical Laboratory (NPL), Hampton Road, Teddington, Middlesex TW11 0LW, United Kingdom.*

[2]*Centre for Research on Adaptive Nanostructures and Nanomaterials (CRANN), School of Physics, Trinity College Dublin, Dublin 2, Ireland.*

*Corresponding Author
Telephone number: +44 20 8943 6434
Email address: toby.sainsbury@npl.co.uk

Abstract: We report the covalent functionalization of exfoliated boron nitride nanosheets (BNNSs) using dibromocarbene (DBC) species. The functionalization of BNNSs is enabled as the nanosheets are utilized as 2-dimensional (2-D) phase-transfer catalysts (PTC) for the migration of carbenes across the organic-aqueous phase boundary. We postulate that BNNSs stabilize carbenes by forming B-CBr_2 ylides and in-turn act as the reaction substrate. DBC functionalization of BNNSs results in the formation of B-C and B-N bonds to the sp^2 hybridized BNNS lattice *via* the formation of dibromo-bridged bicyclo BCN systems. The covalent functionalization was characterised using HR-TEM, AFM, EELS, XRD, EDX, ToF-SIMS, TGA, Raman, XPS, FTIR, and UV-Vis techniques. Utilization of CBr_2 groups as a means by which BNNSs may be integrated and interfaced with solvents, molecular and condensed phase materials was demonstrated by grafting alkyl chains from the functional groups *via* alkyl/halogen exchange. Alkyl-functionalized BNNSs were integrated within polyethylene (LDPE) and extruded to form BNNS-nanocomposite fibres. Implications of the covalent functionalization of h-BN are considered in the context of band-gap manipulation and the versatility of the CBr_2 functional groups to enable subsequent chemical derivatization.

Introduction

In recent years, the exfoliation of 2-D layered materials has been achieved using mechanical, chemical and electrochemical techniques to produce single and few atomic layer nanosheets.[1-3] While electronic, magnetic and optical devices require patterning and the design of suitable contact geometries to efficiently probe their properties,[4] other applications for mechanical, thermal and complex 3-D architectures will require chemical compatibility to interface with solvents, molecular species and condensed phase substrates. Hence, the ability to firstly exfoliate and then secondly chemically modify the surface of nanosheets in a controlled fashion offers viable processing routes towards technological applications such as nanocomposites, electronics and energy storage, catalysis, sensing and diagnostics.[5,6] In the case of graphene converted to graphene oxide (GO); the ability to graft alternative chemistries to oxygen functional groups (-OH, C=O, -COOH) has facilitated enormous expansion of the application of GO and highlights the benefit of tuneable surface chemistry for the dispersion and integration of GO within solvent, molecular and condensed-phase systems.[7,8]

In view of the demonstrated potential of graphene oxide,[8] research efforts have grown to focus attention on the chemical modification of alternative 2-dimensional nanomaterials such as exfoliated BNNSs,[9-12] which is structurally analogous to graphene and possesses a range of similarly attractive intrinsic attributes. Exfoliated BNNSs are electrically insulating, transparent/white, exhibit high thermal conductivity, extreme chemical stability, high mechanical strength, and offer barrier and membrane function as a result of the extended 2-dimensional configuration of the sp^2 hybridized lattice. [13-15]

Approaches which have imparted chemical functionality to both carbon nanotubes (CNTs) and graphene such as oxidative and radical based functionalization have facilitated enormous expansion of strategies for the chemical integration and application of these materials over the last number of decades.[16,17] Comparatively, the covalent functionalization of boron nitride systems has been limited on account of both high chemical stability and hydrophobicity of BN materials within reactive organic and aqueous systems. This has prompted the use of highly reactive radical based functionalization strategies to impart chemical functionality to these materials. BNNTs have been covalently functionalized with amine and hydroxyl groups using radicals generated using plasma, and in the vapour phase.[18] Such functionalization approaches have in-turn identified the feasibility of subsequent derivatization of initial functional groups and therefore shown the potential for the development of extensive functionalization methodologies for boron nitride materials.[19]

A principle motivating factor for the surface functionalization of nanomaterials is the ability to integrate and compatibilize functionalized nanomaterials within solvent, molecular and condensed phase systems. In the case of carbon based systems, the use of doping and covalent functionalization strategies have highlighted the additional potential for modification to the intrinsic material properties such as carrier mobility, electronic band gap and magnetic states.[20-22] Theoretical reports have also investigated the viability of band-gap manipulation and the influence of ad-atoms on the magnetic states in BN nanomaterials and have indicated significant scope for covalent functionalization strategies.[22-24] In view of this, the use of radical-based functionalization strategies for BNNSs is particularly attractive to controllably introduce chemical functional groups yet retain the principle structural integrity and yet potentially manipulate the electronic and magnetic properties.

In this context, a number of theoretical reports have predicted the susceptibility of BNNS and BNNT substrates to covalent functionalization *via* carbenes: Su and co-workers have described energetically favourable cycloaddition across the B-N bond to form an open double 7 membered-ring (7MR) structure.[25] Subsequent reports by Li and Cao investigated the mechanistic viability of carbene functionalization of BNNTs and BNNSs *via* the formation of open (7MR) and closed cyclopropane (3MR) formation.[26,27] Notably, it was also found that carbene functionalization resulted in modification of the band structure by decreasing the band gap at variable levels of functionalization and substituent species.[26,27] It was postulated that such covalent manipulation could be used to influence the electronic properties of BN nanomaterials from insulators to excellent semiconductors. This hypothesis was further reaffirmed by Kakkar et al, who reported both the energetic and electronic effects of carbene functionalization on BNNT and BNNS substrates.[28] Of particular interest to this work is that the description of halogenated carbene species includes the energetically viable binding of $:CBr_2$ radical species. On this basis, there exists much potential to experimentally validate theoretical predictions which may provide a means to manipulate intrinsic electronic properties of BN nanomaterials and to facilitate their dispersion and

integration within molecular and condensed phase systems. We set out to achieve this by generating reactive carbenes in the presence of solution exfoliated BNNSs.

In this work, we build on our previously reported covalent functionalization of BNNSs using oxygen and nitrene radicals by developing a solution phase methodology for carbene functionalization.[11,12] We report carbene functionalization of exfoliated BNNSs under phase transfer conditions across a bi-phasic solvent interface. BNNSs were exfoliated in an organic phase followed by base hydrolysis of bromoform to generate dibromocarbene (DBC) radicals in the presence of BNNSs. Carbene functionalization of the BNNSs proceeded *via* nucleophilic addition to B-N bonds to form DBC-functionalized BNNSs (DBC-BNNSs), as depicted in Scheme 1.

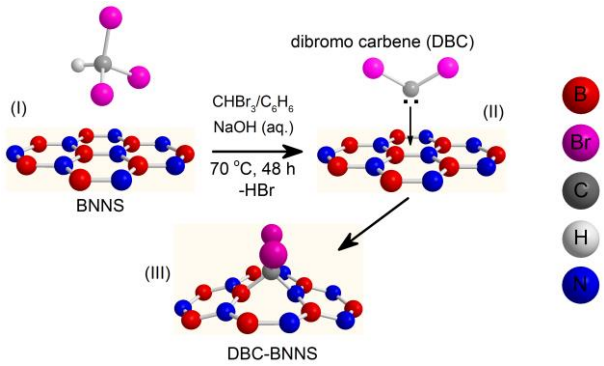

Scheme 1. Dibromocarbene (DBC) functionalization of exfoliated BNNSs (DBC-BNNSs).

By the approach described here, dibromo functional groups were covalently bound to the surface of the BNNSs which were then be used for subsequent covalent derivatization. The covalent functionalization and intrinsic chemical structure was characterized using HR-TEM, EELS, AFM, XRD, EDX, ToF-SIMS, TGA, FTIR, XPS, Raman, and UV-Vis. A notable feature of this work is that, unlike the procedure employed for the bi-phasic carbene radical generation which typically utilizes a tertiary amine as a phase-transfer catalyst, in this work, this procedure has been modified to deliberately exclude this catalyst. We postulate that the BNNSs serve as planar arrays of B atoms, which act as Lewis acids and mediate both the stabilisation of the dibromocarbene and its migration across the phase boundary. To the best of our knowledge this work represents the first experimental report of both carbene functionalization of BNNSs and associated catalytic function.

Experimental

General

Chemicals and reagents used were purchased from Sigma Aldrich and were used as received. Hexagonal Boron Nitride (h-BN) powder (TECO20051158) was generously supplied as a sample from Momentive Performance Materials, Germany. Sonication was carried out using Branson 2510EMT sonic bath. High Resolution Transmission Electron Microscopy (HR-TEM) images and electron energy-loss spectroscopy (EELS) spectra were acquired using a FEI Titan^{TM} 80-300 S/TEM operated at 80 kV. Selected area electron diffraction patterns were acquired using a JEOL-2010 operated at 200 kV. Samples were prepared by evaporating a drop of a dilute suspension of suspended BNNSs onto a lacy-carbon copper TEM grid. AFM measurements were made using an Asylum research MFP-3D system in tapping mode using PPC-NCHR silicon cantilevers at a resonant frequency

of 330 kHz and a force constant of 42 N/m. FT-IR measurements were recorded using a Nicolet 6700, with a diamond ATR accessory. Raman spectra were recorded using a Renishaw inVia Raman Microscope at $\lambda = 514.5$ nm laser excitation. X-ray Photoelectron Spectroscopy (XPS) was performed using a Kratos Axis Ultra DLD system using an Al monochromated X-ray source operated at 15 kV, 5 mA emission. Analysis conditions used were 160 eV pass energy, 1 eV steps, 0.2 sec dwell per step and 2 sweeps. Samples were prepared by evaporation of BNNS material from solution onto Si-wafer substrates. X-ray diffraction measurements were conducted using a Siemens D5000 diffractometer in conjunction with a Cu-kα X-ray tube (40 kV, 40 mA) filtered using a Ni filter and anti-scatter and divergences slits of 1mm under standard θ-2θ conditions. Energy Dispersive X-ray (EDX) analysis was performed using an FEI Sirion SEM in conjunction with an Oxford Instruments EDX detector. ToF-SIMS analysis was performed in the negative ion mode using a ToF-SIMS IV mass spectrometer (IONTOF) with a 25 keV Bi_3^+ primary ion source, a target current of 0.125 pA, and with a final ion dose of 8.2×10^{10} ions per cm^2. Optical Absorption measurements were recorded using a Perkin Elmer Lambda 850 using a 2 mm path-length quartz cuvette. Thermogravimetric Analysis (TGA) was performed using a Perkin-Elmer Pyris-1 TGA system in air. The temperature was scanned from 30 to 1100 ^oC at 10 ^oC/min. Polymer and nanocomposite fibres were prepared using a Ray-Ran 5 series advanced melt flow system (Model 5MPCA). Tensile analysis on fibres was carried out using a TA Instruments RSA-G2 system with a strain rate of 5 μm/min.

Preparation of Dibromocarbene Functionalized Boron-Nitride Nanosheets (DBC-BNNSs)

BNNSs were exfoliated according to a derivation of a published procedure.[2] This involved bath-sonication of h-BN in benzene (20 g, 2.56×10^{-1} mol) in a round-bottomed flask (50 mL) at an initial concentration of 3 mg/mL for 48 h. This was accompanied by cooling using an immersion cooler in order to maintain ambient solution temperature (25 ^oC) and prevent decomposition and/or pressure build-up. This was followed by the addition of bromoform (10 mL, 1.14×10^{-1} mol) to the dispersion and a further period of sonication to ensure complete mixture (2 h). The suspension was then centrifuged at 1500 rpm for 45 mins to remove any aggregated material. The suspension of exfoliated BNNSs was equilibrated for 24 h to allow any insoluble material or aggregates to precipitate. The translucent milky white supernatant fraction (18 mL) was retained and was added drop-wise to a stirring aqueous solution of sodium hydroxide (5 g, 1.25×10^{-1} mol) and allowed stir for 48 h at 70 ^oC. The organic phase was retained and filtered using membrane filtration apparatus (Whatman, Anodisc 200 nm). The residual solid product was then washed with toluene (500 mL) and tetrahydrofuran (500 mL) and was then re-suspended in toluene (30 mL). The organic phase was washed a further three times using water (distilled, deionized, 18.2 M.Ω.cm) and was dried over calcium carbonate (5 g). The retained organic phase containing the suspended dibromocarbene-functionalized BNNSs (DBC-BNNSs) was evaporated to dryness and stored under vacuum for several days for subsequent analysis using Schlenk apparatus. A control experiment was run under identical conditions to the DBC functionalization above with the absence of the dibromocarbene precursor; bromoform.

Preparation of Butyl Functionalized BNNSs (Bu-BNNSs)

Organolithium reagent, n-butyl lithium (n-BuLi) was employed in this work in order to alkylate DBC-functionalized BNNSs. It is noted that n-BuLi is an extremely reactive reagent, and as such careful planning prior to execution of the experiment was carried out. Suitable personal protective equipment was identified and

utilized. N-BuLi was used under air and moisture free conditions using schlenk vacuum apparatus and was quenched and disposed of appropriately. n-BuLi(0.8M in hexane)(50 mL) was added to DBC-BNNSs (50 mg) under oxygen-free conditions. The mixture was sonicated to suspend the nanosheets within the n-BuLi solution to ensure reaction between the n-BuLi and the DBC groups. The reaction mixture was allowed to stir for 48 h. n-BuLi was then quenched by the sequential addition of anhydrous methanol (200 mL). The reaction mixture was then filtered using membrane filtration assembly in conjunction with Whatman, Anodisc^{TM}, alumina filters (0.2 μm), followed by washing with anhydrous methanol (300 mL) and anhydrous dichloromethane (300 mL). The dry butyl-functionalized BNNSs (Bu-BNNSs) product was retained for analysis.

Preparation of Bu-BNNS Polyethylene (Bu-BNNS:PE) Nanocomposite Fibres

Bu-BNNS:PE nanocomposite material was formed by the dispersion of the BNNSs in a large solvent excess followed by gradual addition of PE and subsequent solvent extraction. Bu-BNNS (50 mg) was dispersed in toluene (500 mL) using bath sonication for 2 h. The dispersion was refluxed at 130 ^{o}C followed by the gradual addition of PE (50 g) over a 6 h time interval. Upon final addition of the PE, the carrier solvent, toluene, was removed by distillation followed by rotary evaporation and finally using a vacuum oven (48 h, 30 ^{o}C, 7.5×10^{-3} Torr). This procedure was repeated using PE in the absence of any nanomaterial filler to form a control material under identical conditions. Solid PE and Bu-BNNS:PE materials were extruded using a heated barrel extrusion apparatus (RayRan, 5MPCA) at 180 ^{o}C through a 1 mm die. Fibres were hot drawn to yield narrow fibres of uniform diameter, this was accompanied by a transition from an opaque to a transparent appearance as fibres were drawn which indicates the alignment of the polymer chains. Fibres were cut into 10 cm sections and stored in a vacuum oven prior to analysis.

Results and Discussion

Solution-phase exfoliated BNNSs were prepared using an exfoliation protocol reported by Coleman and co-workers.[2] In this work, the procedure involved sonicating bulk h-BN powder in a benzene/bromoform mixture to reduce the stacking of the nanosheets within the bulk h-BN crystallites. Following the sono-mechanical exfoliation, the distribution of the sheet count between mono-layer to bulk crystallites is refined by centrifugation to yield optimal exfoliated nanosheets of few-layer to mono-layer BNNSs. Retention of the supernatant fraction following centrifugation yields single and few layer sheets in solution and present optimum surfaces for covalent chemical functionalization. Carbene radical functionalization of the exfoliated BNNSs was carried out using a derivation of synthetic procedures based on the hydrolysis of halogenated carbene precursors.[29] Notably, in procedures developed by both Makosza and Kimura the use of tertiary amine molecules as phase-transfer catalysts (PTC) in bi-phasic aqueous-organic mixtures is essential for the formation of cyclopropyl rings at alkene substrates.[30,31] and has also been utilized to functionalize CNTs and graphene with dibromo- and dichlorocarbene respectively.[32,33] In the absence of the PTC, carbenes are readily quenched at the solvent interface and no product is formed. In the work reported here, analogous to alkene and sp^2 hybridized carbon substrates, the bi-phasic procedure is used, however the tertiary amine PTC is deliberately omitted as the concept of the BNNSs acting as catalytic phase-transfer agents is introduced. The rationale for this approach is that BNNSs provide planar arrays of electron deficient B atoms which act as Lewis acids/electron acceptors. B atoms thus facilitate the stabilization of the carbene intermediate by ylide formation.

Carbenes stabilized in this manner are then able to covalently bind to B-N bond pairs to functionalize the sp^2 hybridized h-BN lattice.

Following dibromocarbene (DBC) functionalization, HR-TEM and AFM were used to characterize the integrity of the DBC-BNNSs. Figure 1a shows a TEM micrograph of multiple DBC-BNNSs on a lacey carbon film TEM grid and indicate that the typical lateral dimensions of the nanosheets are of the order of 1-2 μm. Figure 1b shows a typical isolated nanosheet and identifies the 2-D structure of the BNNS. Electron diffraction performed on the isolated nanosheet confirms the hexagonal atomic structure and hence the sp^2 hybridization of the DBC-BNNS lattice, Figure 1c. Both the TEM micrographs and the diffraction data thus confirm that the structural integrity of the nanosheets remains intact following the reaction procedure. AFM was used in order to determine the thickness of individual exfoliated DBC-BNNSs deposited onto a silicon wafer substrate, Figure 1d. Scanning across the edge of the nanosheet identifies a mono-layer with a thickness of 350 pm.

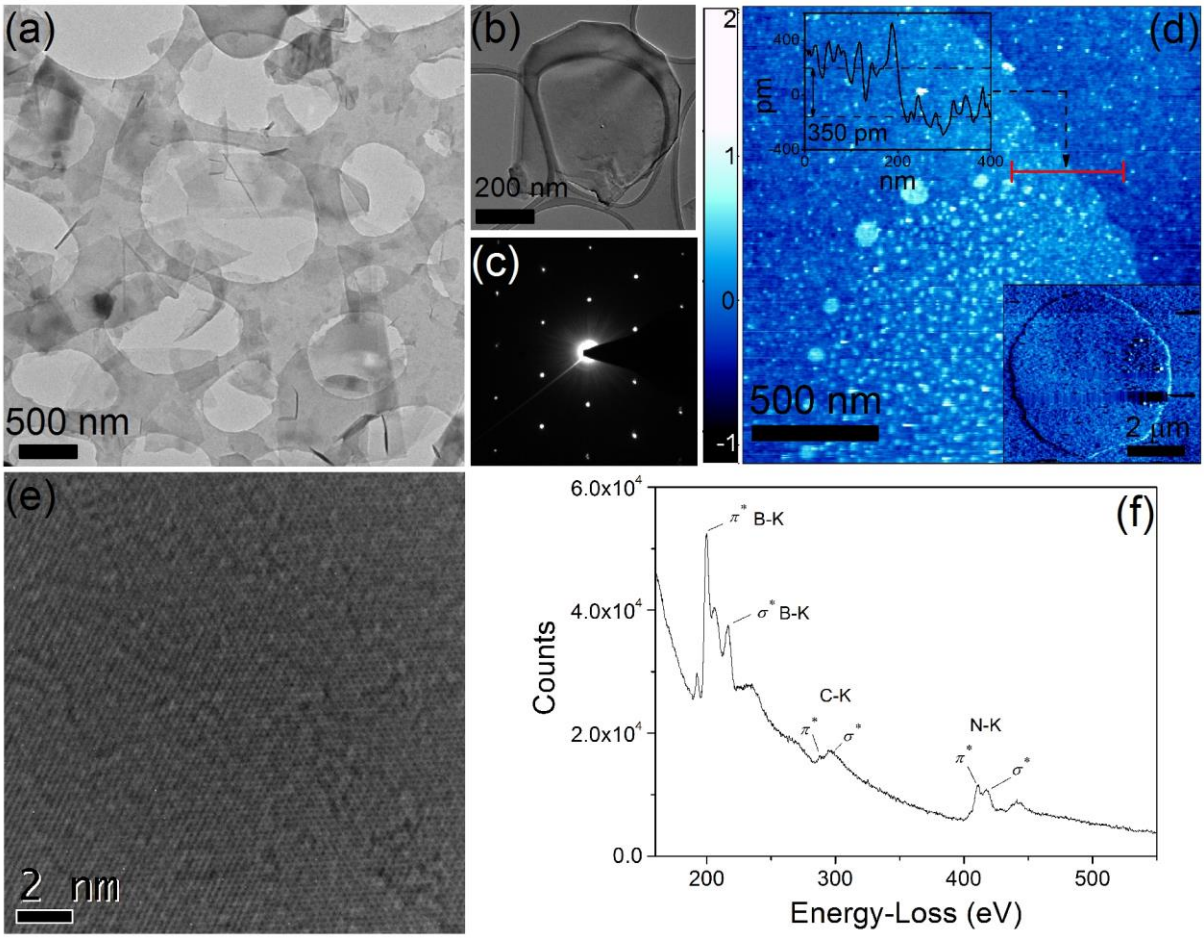

Figure 1. (a) TEM micrograph of exfoliated DBC-BNNSs at low magnification. (b) Individual DBC-BNNS showing typical representative dimensions (~1 μm × 1 μm). (c) Electron diffraction pattern indicating the hexagonal lattice structure of a suspended DBC-BNNS. (d) AFM image of an isolated mono-layer DBC-BNNS, thickness ~350 pm. (e) HR-TEM micrograph indicating lattice structure of a DBC-BNNS. (f) EELS spectrum of a suspended DBC-BNNS indicating the principle K-shell excitations; B, C and N.

A high magnification image of an isolated nanosheet indicates that the lattice structure of the nanosheets is intact and free from large defects, which may occur from sono-mechanical energy or by an unzipping of the h-

BN lattice following the covalent functionalization, Figure 1e. In the case of graphene oxide where sheets display large voids it is encouraging that the reactive chemical process used here does not cause any noticeable holes and distortions to the structure of the BNNSs.

Electron Energy Loss Spectroscopy (EELS) identifies the K-shell ionization edges starting at 185 eV and 393 eV which correspond to B and N respectively which are comprised of the 1s-π^* and 1s-σ^* anti-bonding orbitals, Figure 1f. Notably in the EELS spectrum, peaks beginning at 274 eV indicates the presence of the C-K edge. The peak corresponds to the 1s-σ^* anti-bonding orbital centred at 296 eV. This peak is in agreement with literature values for the C-K edge within sp^2 hybridized BCN domains.[34] The presence of the single peak C-K edge following functionalization suggests the presence of CBr_2 species bound to the BNNSs. This is in contrast with spectra of pristine sp^2 hybridized BNNTs, [35,36] and the BNNS control sample in this work, which are featureless in the region of the C-K edge at ~290-320 eV (Supporting Information, Figure S1). The EELS spectrum of DBC-BNNSs additionally exhibits a defined Br-M edge at 71 eV which is assigned to CBr_2 groups covalently bound to the h-BN lattice (Supporting information, Figure S2). Under high vacuum conditions for analysis, identification of both C and Br is indicative of covalent chemical functionalization rather than the presence of starter material residues.

In view of the typical stability of BNNSs to reactive chemistries, the characterization of the covalent DBC functionalization of the BNNSs consisted of three phases as follows: The presence of the CBr_2 adduct species was identified using XRD, EDX, and ToF-SIMS techniques, and quantified using TGA. This was followed by the use of spectroscopy; FTIR, Raman, and XPS to determine the nature of the CBr_2 bonding to the h-BN lattice. Finally, UV-Vis spectroscopy was employed to assess the modification of the intrinsic optical energy transitions as a result of the covalent functionalization.

XRD analysis was performed on both pristine BNNSs and DBC-BNNSs to characterize the covalent functionalization, Figure 2a. In the spectrum of the pristine BNNSs the (002) crystallographic plane is located at 27.01^o while peaks at 42.12^o, 43.54^o, 50.73^o, and 55.82^o are indicative of the (100), (101), (102), and (004) planes respectively (Figure 2a).[35,37] Following DBC functionalization, the (002) peak has shifted by 0.08^o to 27.09^o (Supporting information, Figure S3). The shift is accompanied by the addition of a number of peaks identified as reflections of B-C bonding at 35.03^o, 37.95^o, 40.61^o, and 48.00^o and C bonding at 43.10^o and 45.65^o.[38]

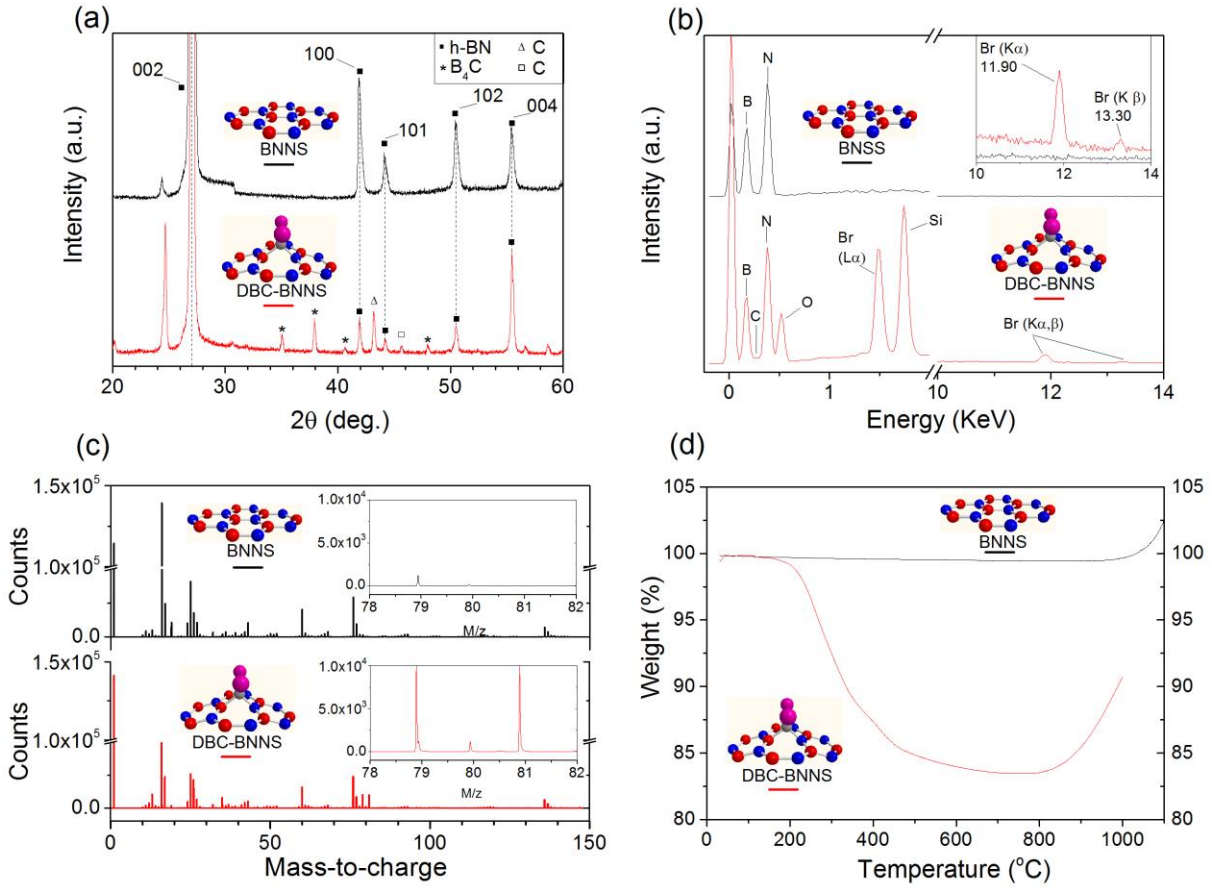

Figure 2. (a) XRD spectrum of BNNSs and DBC-BNNSs showing additional B-C and C peaks following functionalization. (b) EDX spectra of BNNSs and DBC-BNNSs. Inset showing increased intensity 10-14 KeV region. (c) ToF-SIMS spectra of BNNS and DBC-BNNS samples in mass/charge range 0-150 and insets showing BNNS and DBC-BNNS in the mass/charge region for the Br2+ ion 78-82. (d) TGA trace for BNNSs and DBC-BNNSs exhibiting mass loss of DBC groups between 200-400 ^{o}C.

The elemental composition of the DBC-BNNSs material was characterized using EDX analysis, Figure 2b. Relative to the spectrum of the pristine h-BN material, the spectrum of DBC-BNNS exhibits strong peaks due to Br Lα at 1.5 KeV and at 11.90 KeV and 13.30 KeV corresponding to the Br Kα and Kβ emission lines respectively. The inset in Figure 2b shows the region from 10-14 keV at higher intensity and shows the Br Kα and Kβ peaks of the DBC-BNNSs relative to the pristine BNNS. Si and O peaks are due to the SiO_2/Si substrate. Time-of-Flight Secondary-Ion Mass Spectroscopy (ToF-SIMS) was also used to identify CBr_2 groups on the surface of the DBC-BNNSs. This technique has previously been used to identify Br-functionalization of graphene nanoplatelets (GNPs) by analysis of the intensity ratio of the isotopic peaks due to atomic Br at molar masses of 79 and 81.[39] In this case; ToF-SIMS analysis indicates the presence of bromine in the DBC-BNNSs, Figure 2c. Bromine has two stable isotopes that are two mass units apart and relatively equal in abundance (^{79}Br, 50%) and ^{80}Br, 49%). The ToF-SIMS spectrum of DBC-BNNSs clearly shows the bromine anion isotopes at m/z 78.92 and m/z 80.92, Figure 2c. The integrated, Poisson-corrected, and background subtracted intensities for these peaks were 1.81×10^5 and 1.85×10^5 counts, which calculates to a relative abundance of 49.4% and 50.5%, respectively which validates the assignment of the bromine dimer (Br_2^+). The mass deviation for expected mass of the bromine isotopes was 3.6 ppm for the ^{79}Br isotope and 12.8 ppm for the ^{80}Br isotope.

Bromine peaks were absent in the pristine BNNS control sample (Figure 2c) and confirms the addition of the bromine adducts to the BNNSs following the DBC functionalization. TGA was used to quantify the DBC adducts covalently bound to the BNNSs. The TGA trace of the DBC-BNNSs exhibits significant mass loss of approximately 16% of the total sample between 200-450 ^{o}C indicative of the loss of the CBr_2 groups. Following the initial loss of functional groups, thermal decomposition of the functionalized nanosheets structure is observed at ~800 ^{o}C.[40] This lower degradation temperature occurs due to disruption of the BNNS lattice following functionalization and thus creates defect points which serve to accelerate the thermal decomposition of the DBC-BNNSs relative to the pristine BNNS. The proportion of CBr_2 functional groups at the surface of the DBC-BNNSs, 16%, is equated to a functionalization density of ~1.33 at.%. This may be expressed as one DBC functional unit per 75 atoms in the h-BN lattice, which is calculated to be one DBC group per 1.6 nm^2, (Supporting information, Figure S5). Considering a typical 1 μm^2 nanosheet, functionalization density would be therefore yield 1×10^6 groups per sheet and thus 0.5×10^6 DBC functional units per side. In terms of integrating with solvents systems or facilitating anchoring of polymer chains or catalytic nanoparticles, this number is satisfactory considering that the functionalization reaction retains the basic intrinsic lattice structure and hence intrinsic material properties.

DBC-Functionalization of BNNS has been confirmed using EELS, XRD, EDX, ToF-SIMS, and TGA. Fourier Transform Infrared spectroscopy (FTIR), Raman spectroscopy, and X-ray Photoelectron-Spectroscopy (XPS) were then used to characterize the bonding between DBC groups and the sp^2 hybridized BN lattice.

FTIR analysis of DBC-functionalized-BNNSs was performed by comparing spectra for the pristine starting h-BN material, the reagent bromoform and the DBC-BNNSs. Prior to functionalization, pristine BNNSs exhibit characteristic in-plane h-BN ring (E_{1u} mode) and out-of-plane h-BN (A_{2u} mode) vibrational modes at 1370 cm^{-1} and 810cm^{-1} respectively, Figure 3a.[36,41] The FTIR spectrum of the bromoform molecule, Figure 3b, exhibits alkyl C-H stretching and bending bands at 3020 cm^{-1} and 1142 cm^{-1} respectively. Asymmetric and symmetric CBr_2 bands are evident at 692 cm^{-1} and 656 cm^{-1}, while the lesser band at 540 cm^{-1} is assigned to the CBr_2 wagging vibration. In the spectrum of the DBC-BNNSs, the appearance of bands corresponding to B-C, C-N and C-Br bonds indicate the covalent binding of the carbene species to the h-BN lattice (Figure 3c). The formation of the B-C bond is confirmed by the appearance of a strong band at 1150 cm^{-1} which corresponds to the E_{1u} B-C stretching mode,[42-44] while the strong shoulder band at 1078 cm^{-1} is indicative of the C-N bond.[42] Concomitant formation of both B-C and B-N bonds indicates the formation of a BCN heterocyclic structure as the carbene group binds to both B and N atoms in the BNNS lattice to satisfy its unpaired electron pair.

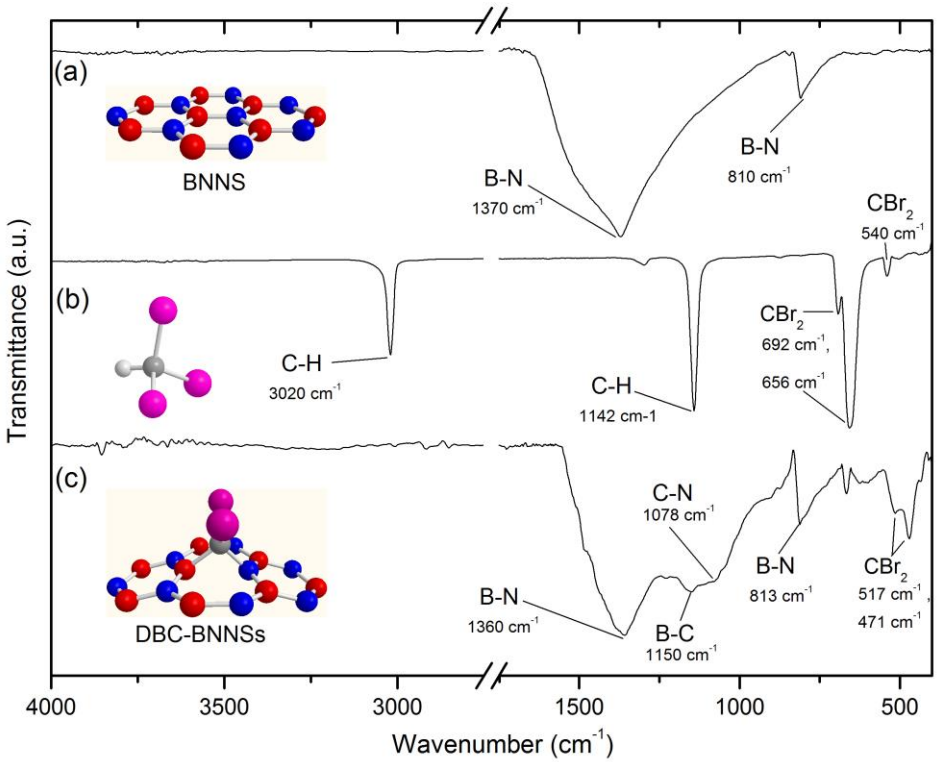

Figure 3. FTIR spectra of (a) pristine BNNSs, (b) bromoform, (c) dibromocarbene-functionalized BNNSs (DBC-BNNSs).

The signature of C-Br bonds in the carbene group are observed as bands at 517 cm^{-1} and 471 cm^{-1} which are indicative of the asymmetric and symmetric C-Br stretching vibrations.[45] The identification of these bands combined with the evidence of B-C and C-N bands, confirms the presence of DBC groups covalently bound to the BNNSs (Figure 3c). Following DBC functionalization, the E_{1u} in-plane mode at 1360 cm^{-1} has shifted (10 cm^{-1}) from 1370 cm^{-1} in the pristine BNNSs, while the A_{2u} out-of-plane mode at 813 cm^{-1} has shifted (3 cm^{-1}) from 810cm^{-1} in pristine BNNSs. These shifts are in agreement with studies concerning BNNS functionalization using nitrene and oxygen radicals and are indicative of enhanced sp^3 tangential vibrations in the lattice.[11,12,36,41]

Importantly, the FTIR spectrum of DBC-BNNSs is absent of bands corresponding to free bromoform molecules which exhibits alkyl (C-H) stretching and bending vibrations at 3020 cm^{-1} and 1142 cm^{-1}, and the C-Br asymmetric and symmetric stretching vibrations at 692 cm^{-1} and 656 cm^{-1}.[45] The large difference between the free-molecule C-Br bands at 692/656 cm^{-1} and the bound groups 517/471 cm^{-1} confirms the covalent binding of the groups to the BNNSs and precludes the presence of the free bromoform molecules. The combined FTIR analysis confirms the covalent DBC-functionalization of BNNSs *via* the formation of B-C and N-C bonds

Raman spectra of pristine BNNS and DBC-BNNS are shown in Figure 4a. The spectrum of pristine BNNSs exhibits a single peak corresponding to the high frequency intralayer Raman active E_{2g} mode at 1366 cm^{-1} with a FWHM value of ~20 cm^{-1}.[46] Following DBC functionalization, the E_{2g} mode exhibits a FWHM value of ~11 cm^{-1} and has shifted by 2 cm^{-1} to 1364 cm^{-1} which denotes the decreased intra-layer contribution indicative of nanosheet exfoliation.[47] This is accompanied by the appearance of a band at 1086 cm^{-1} indicative of covalent B-C bonding. This is in agreement with reports in the literature concerning the E_{2g} B-C Raman active mode in BC

and BCN films at approximately 1100 cm^{-1} and corroborates the FTIR analysis identifying the B-C bond.[48,49] While the B-C bond is known to exhibit the Raman active E_{2g} mode it is known that the C-N bond is non-polar and is not typically observed in Raman spectra at low concentrations within N-doped boron carbides (< 10-12%) as indicated by studies by Ferrari et al.[50] In this work, at a reasonably discreet functionalization density (< 2%), we therefore do not observe a C-N signal in the Raman spectrum. Additional bands in the DBC-BNNS spectrum at 712 cm^{-1} and 278 cm^{-1} correspond to the ν2, Br-C-Br symmetric stretching mode and the ν4, Br-C-Br bending mode. These values are in close agreement with the theoretical and experimental values reported by Phillips and co-workers and confirm the identification of the DBC group.[51]

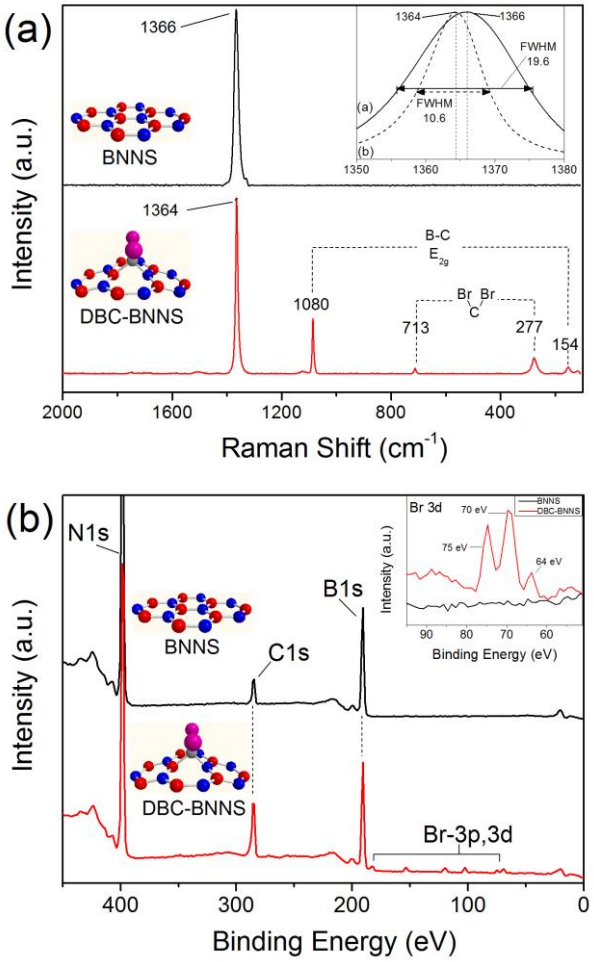

Figure 4. (a) Raman spectrum of BNNS and DBC-BNNS indicating B-C bond formation and CBr_2 groups. (b) XPS survey spectra of BNNS and DBC-BNNS and insert showing Br 3d region at enhanced intensity.

To further evaluate the chemical composition and covalent bonding of the DBC-BNNSs, analysis by XPS was undertaken. Figure 4b shows XPS survey spectra of BNNSs and DBC-BNNSs. In both spectra, the dominant features are the N1s and B1s peaks at approximately ~191 eV and ~400 eV respectively, which are consistent with values reported in the literature for few-layer BNNSs.[52] In the spectrum of DBC-BNNSs, a series of peaks between 50-200 eV corresponding to Br 3p and Br 3d signals are evident. The inset in Figure 4b indicates the presence of the Br 3d bonding in the case of the DBC-BNNSs relative to the BNNSs sample. Analysis of the

B1s core level spectra, (Supporting Information, Figure S6a), shows a symmetric peak centred at 190.6 eV for BNNSs. The over-laid DBC-BNNS B1s spectrum is centred at 190.5 eV and is accompanied by a asymmetric broadening contribution to the peak at lower energy at 190.0 eV. This is assigned to B-C bonding, and has been previously reported for h-BCN hybrid and BCN thin films.[34,42,53] Analysis of the N1s core level spectra for BNNSs indicates a symmetric N1s peak centred at 398.1 eV (Supporting Information, Figure S6b). Analogous to the case of the B1s spectra, the N1s peak for DBC-BNNSs, centred at 398.2 exhibits asymmetric broadening at higher energy, 398.8 eV (Supporting Information, Figure S6b). This is indicative of N-C bonding and has also been previously noted in literature reports describing sp^2 hybridized bonding between B, C and N atoms.[34,42,53] Analysis of the C1s spectrum for DBC-BNNS also identifies a shoulder peak at 287.2 eV assigned to CBr2 and confirms the bonding of the DBC species to the BNNSs.[54] Combined with the FTIR findings, this evidence indicates that both B-C and N-C bonds have been formed with the BNNS lattice and thus supports the assertion of the formation of a BCN heterocyclic structure. Considering the theoretical predictions of carbene functionalization of BNNTs and BNNSs we now speculate on the mechanistic pathway for DBC-functionalization of BNNSs.

Generation of dibromocarbene species are known to occur *via* the base mediated hydrolysis of the carbene precursor; bromoform.[29-31] In this work, we postulate that exfoliated BNNSs in the organic-phase may facilitate the formation of a stabilized B-C ylide reaction intermediate at the phase boundary between BNNSs-B atoms and dibromocarbene generated in the aqueous-phase. BNNS-carbene ylide pairs would form in an analogous manner to ylides formed from dichlorocarbenes and tertiary amines,[31] however in this case, the B atom forms the favourable pathway to stabilize the carbene rather than the electron rich N atom. Subsequent formation of B-C and C-N bonds would result in the cleavage of the B-N bond in the lattice plane. The proposed reaction is summarized in Scheme 2a. The proposed reaction mechanisms is explained by the fact that atoms in the sp^2 hybridized BNNS lattice exist as polar covalent bonds whereby B atoms are electron deficient and therefore possess a partial charge, δ^+, N atoms are electron rich possessing an electron lone pair and thus a partial charge, δ^-. In the case of nitrene and oxygen radical nucleophilic attack, radical species with an unpaired electron attack the electron deficient B atoms which act as Lewis acids and form B-N and B-O bonds respectively; this is accompanied by cleavage of the B-N bond in the lattice plane. In the case of carbene radical attack of the BNNS lattice, where the carbon atom has two unbound electrons, the theoretical energetic viability of a reaction product has been investigated by a number of authors as well as the implications for bonding to the lattice plane.[25-28] Formation of closed three-membered BCN ring structures have been predicted to be energetically unfavourable and are therefore precluded.[26] The formation of open back-to-back seven-membered ring structures incorporating a carbon atom are predicted to be energetically viable and are thus hypothesised to be the relevant mechanistic pathway in this work.[26]

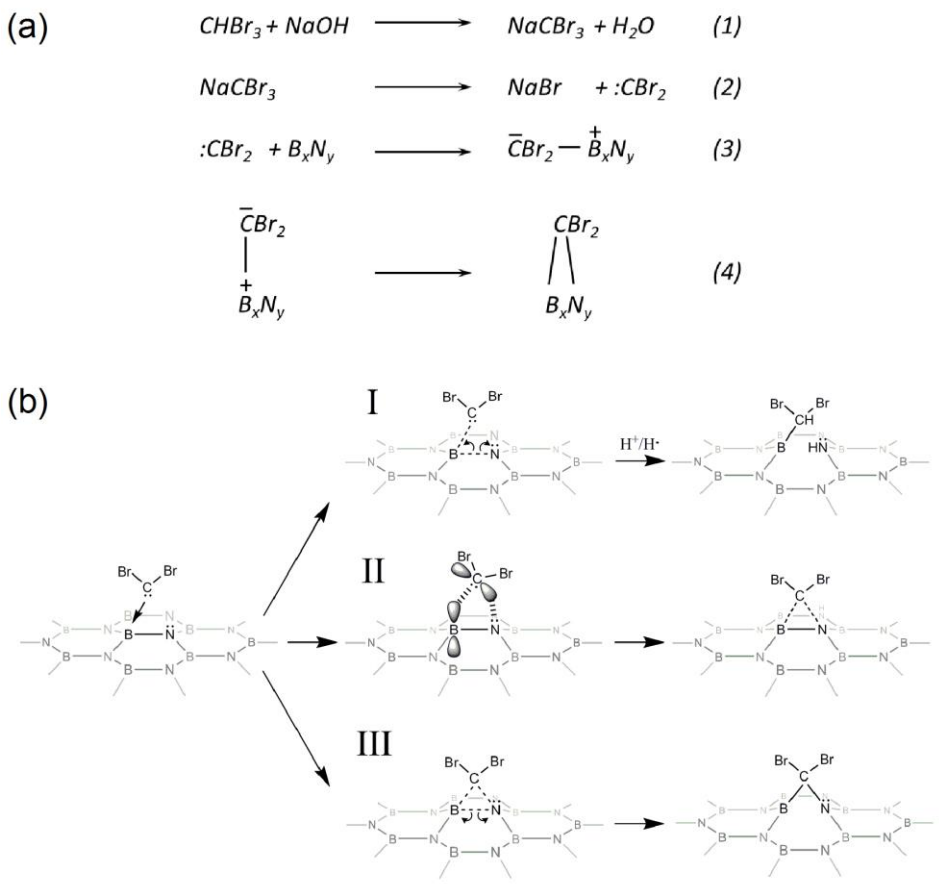

Scheme 2. (a) Generalized reaction mechanism for dibromocarbene functionalization of BNNSs *via* B-C ylide formation. (b) Mechanistic pathways for carbene attack on the BNNS substrate. (I) open, single B-C bonding configuration, with B-N cleavage in the basal plane, (II) closed, 3-membered ring (3MR), transition state bonding configuration, (III) closed, 7-membered ring (7MR), with basal plane B-N bond cleavage and satisfied valence conditions.

To support the assertions made above, firstly, identification of both B-C and C-N bonds from the FTIR and XPS analysis implies that mechanism pathway I in Scheme 2b, is precluded, i.e. carbene attack of the electron deficient B atom. In this scenario, it is envisaged that the B-N bond breaks and to satisfy the valence conditions, the unsaturated carbon and nitrogen atoms would presumably become terminated by scavenging H atoms in the reaction mixture containing H and Br following the dissociation of bromoform. Secondly, considering the spectroscopic data which indicates the formation of both B-C and C-N bonds, this experimental evidence validates the theoretical predictions of a ring structure upon carbene functionalization across the B-N bond. This implies that either a closed three-membered (3M) ring structure is formed in one case, pathway II, or in the third case, pathway III, that a seven-membered (7M) ring structure is formed as the B-N bond is broken and the carbene adds across two back-to-back 7M rings. Considering the theoretical work by both Zhao *et al* and Su describing the formation of the 3M and 7M ring structures,[26] in the 3M ring case, ring formation is predicted to occur by the overlap of the N lone pair electrons with the unoccupied P orbital from the C atom, thus forming a BCN ring structure albeit with unfavourable valence and energy conditions, pathway-II.[25] In the 7M ring case, we propose that the dibromocarbene is stabilized by a B atoms as a ylide intermediate. Upon decomposition, the B-N bond is cleaved while a B-C bond is formed. This in turn facilitates the free N electron to form the N-C bond with the unpaired carbene electron, thus forming the energetically favourable predicted 7M ring structure,

pathway-III. Therefore, when considering the formation of these structures in comparison to the direct insertion reaction, the formation of a ring structure is viable and energetically favourable in the case of the 7M ring structure, pathway III. In contrast, pathway-I, carbene attack on the boron atom, would be limited by the diffusion of H atoms in solution and particularly unfavourable in view of the highly basic reaction mixture the carbene functionalization is carried out in. To confirm the assertion of ring formation, the FTIR spectrum of DBC-BNNSs does not show any C-H or N-H bands indicative of the insertion open structure by single C bond attack (pathway-I), and does show the B-C and C-N bonds which support the formation of the 7M ring structure (pathway-III). FTIR also does not support evidence for the formation of a closed BCN 3M ring with cleavage of bonds tangential to the B-N bond (pathway-II). No FTIR evidence of amine or borane species have been identified (Figure 3c). The hypothesis of B-C and C-N bond formation in an open back to back 7M ring configuration is additionally supported by both XPS evidence which identifies the shifts to the B1s and N1s in identical manner in the energy regions consistent with B-C and N-C bond formation and by Raman evidence which identifies the formation of B-C bonds. Consideration of the FTIR, Raman and XPS characterization validates the theoretical prediction of Zhao *et al* and confirms the assertion that carbene addition occurs *via* the formation of back-to-back 7M rings, pathway-III.[26] Undoubtedly this type of modification to the sp^2 hybridized h-BN lattice induces dislocation of B and N atoms orthogonal to the lattice plane, while the central C atom exits in an sp^3 hybridization state. Since the ring systems must remain intact without dangling bonds, we therefore speculate that the dibromo-carbene bridged bicyclo groups in the h-BN lattice must exist as synthetically induced 7-membered cyclic structures similar to stone-wales defects in graphene.

Analogous to studies involving graphene, where the band gap energy may be increased by doping and surface functionalization,[20-22] in case of BNNSs, an insulator with a band gap of 5.56 eV,[14] it has been predicted that covalent functionalization by carbene species may lower the band gap to 0.6 eV.[23] UV-Vis spectroscopy has been used by a number of authors to investigate the optical energy gap of h-BN thin films.[46,52] To investigate modification to the optical energy gap in BNNSs following DBC functionalization, UV-Vis spectroscopy was performed on dilute suspensions of both BNNSs and DBC-BNNSs. For dilute nanosheet suspensions, the band edge is observed as an independent peak and differentiated from the scattering edge of higher concentration suspensions and thin-films.[2,46,52] The wavelength of the band edge peak, λ_g (the optical band gap wavelength) corresponds to E_g, the optical band gap energy, where $E_g = hc/\lambda$, therefore modification to the optical band gap following functionalization is investigated by analysis of the band edge peak position.

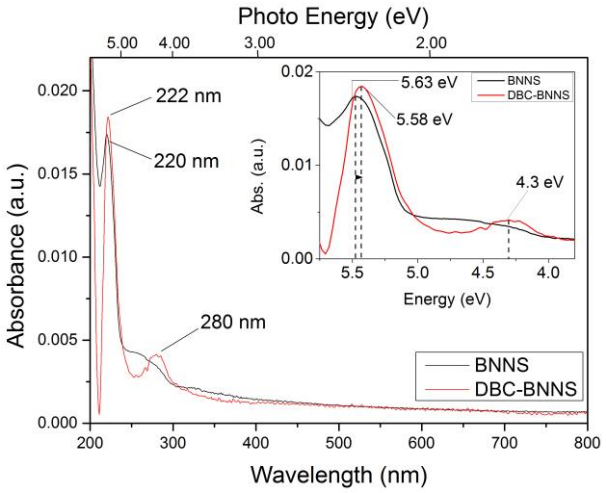

Figure 5. UV-Vis spectra of exfoliated BNNSs (black) suspension and DBC-BNNS (red) in 2-propanol.

Figure 5 shows background subtracted UV-Vis spectra for exfoliated BNNSs (black) and DBC-BNNSs (red) .The spectrum for BNNSs shows the profile for the pristine material at high dilution. Suspensions of BNNSs at higher concentrations typically exhibit a scattering profile at lower wavelength (<350 nm). Upon dilution, a faint profile of a discreet absorption edge may be observed in the region of the scattering onset (<250 nm). In this case, characterization at ultra-low sample concentrations allows qualitative analysis. Typical sample additions of 1 μL, ca. 0.1 $\mu g.mL^{-1}$, allow the absorption edge of BNNSs to be observed as a defined shoulder peak of the scattering onset which is located at 220 nm, corresponding to an optical band gap of 5.63 eV (Figure 5). This value is in close agreement to a report concerning determination of the optical band gap (E_g) of a thin h-BN film (2-5 layers) using extrapolation of the Tauc function which exhibits a linear absorption edge in the $\varepsilon^{1/2}/\lambda$ vs $1/\lambda$ plot, yielding an optical band gap, E_g, at 5.56 eV corresponding to 223 nm.[46] The Tauc function typically defines the optical band gap in amorphous semiconductors, however in this case, we observe breakdown in the Tauc function in the case of atomic crystalline nanosheets, where non-linearity at the absorption edge precludes any assignment of E_g by extrapolation (Supporting Information, Figure S7). This feature also confirms that exfoliated BNNSs deviate from the absorption behaviour typically observed in few-layer h-BN.[2,12] Following DBC-functionalization, the profile of the absorption edge is modified to a symmetrical sharp peak and has shifted 2 nm to 222 nm, which corresponds to an energy band gap of 5.58 eV, Figure 5. This is also accompanied by the appearance of a second defined absorption edge at 280 nm which corresponds to 4.30 eV. This is almost identical to the report by Ajayan *et al* concerning CVD deposited BCN hybrid films which identified the presence of a hybrid absorption edge at 4.48 eV assigned to C doping within h-BN domains.[34] From the UV-Vis analysis, we believe this hybrid absorption edge observed in Figure 5 (also additive spectra in supporting information, Figure S8), represents an impurity state introduced by the DBC-functionalization to the BNNS lattice. This finding offers experimental validation for the theoretical predictions concerning the modification of the electronic and magnetic states in BNNSs and strongly supports the potential of functionalization mediated band gap manipulation for BN nanomaterials.[9,22,23]

In addition to the modification of intrinsic material properties, a principle motivating factor for the development of chemically functionalized nanosheet materials is that surface chemistry dictates the interaction of nanosheets

within solvent systems, polymer matrices and condensed phase materials. This feature provides a means by which the application of these 2-D nanosheets may be greatly enhanced. Therefore by imparting chemical functionality to BNNSs, chemical groups may be utilized to enable dispersion or to facilitate further chemical derivatization to chemistries specific to an intended technological application. We have demonstrated this concept by chemically derivatizing DBC-BNNSs. Bromine is a versatile intermediate in organic synthesis and is known to undergo exchange with alkyl lithium compounds.[55] Utilizing alkyl-halogen exchange reaction protocol based on aryl-bromide and alkyl lithium species,[55] DBC-BNNSs were treated with n-BuLi in order to facilitate alkyl-bromo exchange. Butyl groups were introduced to the surface of the DBC-BNNSs, to yield butyl-functionalized BNNSs (Bu-BNNSs). The reaction mechanism is described in the supporting information. (Supporting Information, Figure S9). The alkylation of the BNNSs is targeted in view of integration with alkyl based polymer systems such as polyethylene (PE). A growing number of reports in the literature have indicated the potential for BNNSs as a nanofiller in composite materials due to its physical attributes such as high mechanical strength, low density, thermal conductivity and radiation shielding potential.[56-58] There is therefore much potential for approaches which impart chemical functionality to BN nanomaterials for dispersion and integration within polymer matrices.[11,12] The alkyl functionalization of DBC-BNNSs to form Bu-BNNSs was characterized using FTIR, Figure 6a. The key features from the FTIR analysis of the DBC-BNNSs (Figure 3c, 6a), identify the B-N bands and the DBC related B-C, C-N and CBr_2 bands. Following butyl-functionalization, asymmetric and symmetric methylene bands of the butyl (C_4H_9) group are evident in the spectrum of the Bu-BNNS at 2925 cm^{-1} and 2850 cm^{-1} respectively (Figure 6a). The appearance of the alkyl bands is accompanied by the disappearance of CBr_2 bands at 517 cm^{-1} and 471 cm^{-1} which indicates that the reaction occurs by Br-alkyl exchange and not simply direct attachment of alkyl chains to the BNNSs. As CBr_2 bands are now absent, this suggests that the reaction was efficient and exchanged the halogen atoms with an optimum yield, if this were not the case both Br and alkyl bands would be observed in the spectrum of the Bu-BNNSs. The butyl groups are therefore expected to be in a di-butyl configuration from the central C atom, for simplicity we refer to the material as Bu-BNNSs. Bands assigned to B-C and N-C bonds at 1150 cm^{-1} and 1078 cm^{-1} in the spectrum of DBC-BNNS are present as well resolved bands in the spectrum of Bu-BNNSs at 1154 cm^{-1} and 1080 cm^{-1}. Enhanced resolution of these bands is attributed to the lower mass of the butyl substituents (2×57 $gmol^{-1}$) relative to the Br atoms (2×79 $gmol^{-1}$) which facilitates greater vibrational freedom of the adduct species. The clear identification of both B-C and C-N bands in the Bu-BNNS system once again validates the formation of the BCN ring species and confirms the reaction pathway proposed for the functionalization (pathway-III, Scheme 2b). FTIR evidence confirms the halogen-alkyl exchange reaction and identifies DBC-BNNSs as viable platforms for versatile chemical derivatization and grafting chemistries.

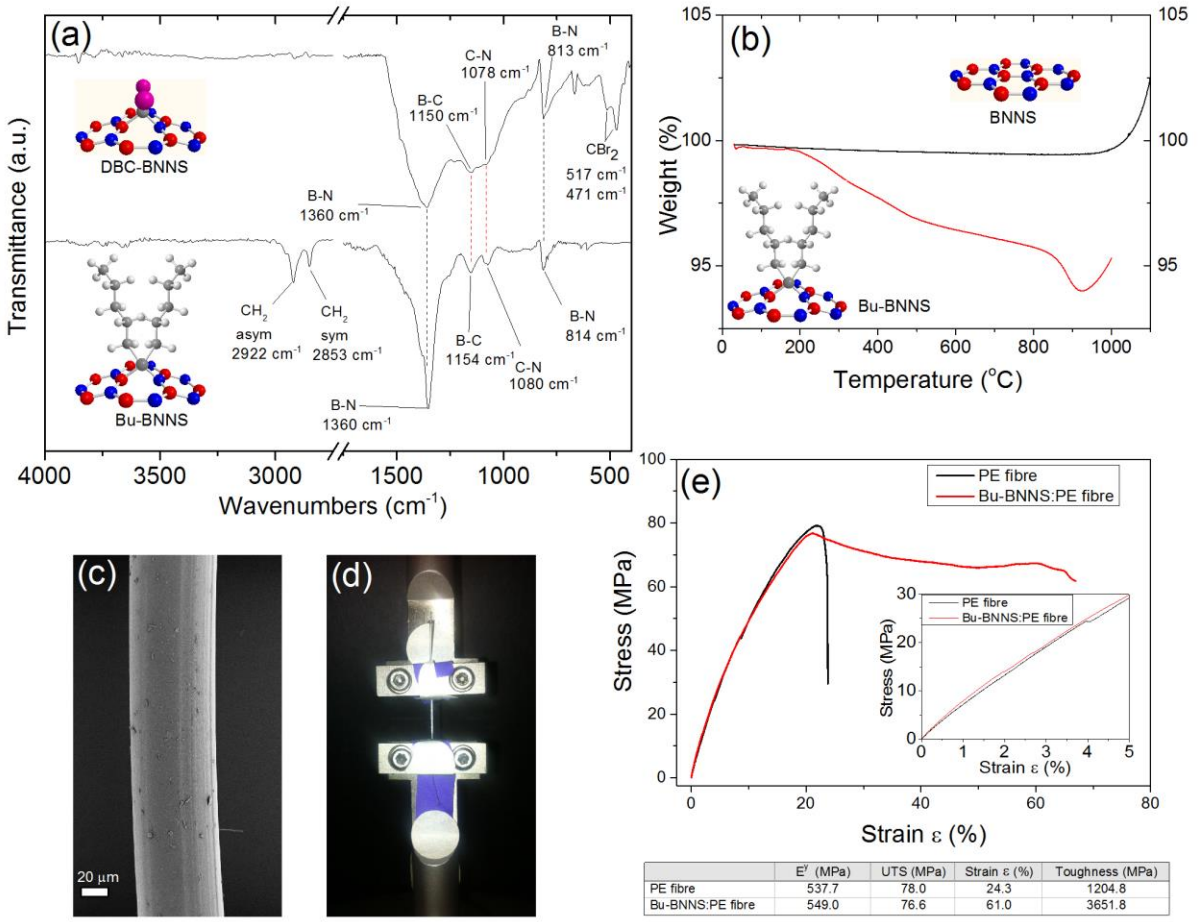

	E^{i} (MPa)	UTS (MPa)	Strain ε (%)	Toughness (MPa)
PE fibre	537.7	78.0	24.3	1204.8
Bu-BNNS:PE fibre	549.0	76.6	61.0	3651.8

Figure 6. (a) FTIR spectra of DBC-BNNSs and Bu-BNNSs, (b) TGA analysis showing decomposition of BNNSs and Bu-BNNSs, (c) SEM image of Bu-BNNS:PE fibre, (d) DMA/micromechanical test rig, (e) tensile test profiles for PE fibre (control) and Bu-BNNS:PE nanocomposite fibre.

To quantify the butyl groups grafted onto the BNNSs, TGA was performed in air, Figure 6b. A mass loss of approximately 7% was recorded for the Bu-BNNSs. The onset for mass loss occurred above 200 ^{o}C which is indicative of the decomposition of the organic ligands, this was then followed by a higher rate of loss above 850 ^{o}C which is speculated to be due to decomposition of the more tightly bound configuration of the carbon groups bound directly to the lattice. Following the decomposition of the functional group structures, mass increase occurred which indicates oxidation of dislocated B atoms to boric acid derivatives.

Having confirmed the butyl-functionalization of the BNNSs, to demonstrate the potential for mechanical reinforcement within a conventional polymer system Bu-BNNSs were dispersed within a low density polyethylene (LDPE) matrix (LDPE hereafter referred to as PE). Bu-BNNS material was dispersed in PE in order to form a nanocomposite at a discrete weight percent loading (0.1 wt.%). Briefly, this involved the dispersion of the Bu-BNNS material in a large excess of toluene which was refluxed to accommodate the gradual addition of PE. Dissolution of PE within a dilute dispersion of the BNNS material allowed optimal integration of the materials. The carrier solvent, toluene, was then extracted using vacuum apparatus to afford the dry nanocomposite product. The solid Bu-BNNS:PE nanocomposite material was recovered and chipped to facilitate loading into a hot barrel extrusion apparatus. At 180 ^{o}C, both PE and Bu-BNNS:PE nanocomposite

fibres were extruded through a 1.0 mm die, and drawn to yield uniform fibres of 0.5 mm nominal diameter, Figure 6c. Fibres were then mounted in a DMA apparatus in a configuration for axial tensile analysis, Figure 6d. Representative stress strain curves for both PE and Bu-BNNS:PE fibres are shown in Figure 6e. Average Young's Moduli, E^y, for the extruded PE fibres and the Bu-BNNS:PE fibres were 537.7 and 549 MPa respectively. Marginally higher values for the h-BN reinforced (Bu-BNNS) PE fibres over pristine PE indicates that the presence of the nanosheets have beneficial rather than detrimental influence over the presumably aligned polymer chains in the drawn fibres and slightly exceed the standard deviation for the data set. The inset in Figure 6e shows the almost identical profile of the initial stages of stress onset. Ultimate tensile strength (UTS) values were 78.0 and 76.6 MPa for the PE and Bu-BNNS:PE fibres respectively which both lie inside the deviation for each data set (1.73, 1.65) and are therefore considered the same. This is contrasted with a significant increase in ductility of the Bu-BNNS:PE fibres over that of the PE fibres, increasing from 23.4 % to 61 %, and with an accompanying increase in the tensile toughness from 1204.8 MPa to 3651.8 MPa. This three-fold increase in the tensile toughness of the fibres is attributed to the impact of the nanosheets which are dispersed within the fibre matrix and chemically compatibilized due to the presence of the butyl chains. It is speculated that the addition of the functionalized nanosheets within the PE matrix prevents slippage between polymer chains as the butyl groups on the h-BN nanosheets act as points to provide entanglement interactions. This restriction in slippage within the fibre matrix would therefore be expected to provide zones which restrict failure mechanisms and thus be exhibited as enhancement in ductility. While it is known that the grafting of longer chains to nanofillers provide enhanced integration with matrices,[11] this preliminary study provides a basis whereby more elaborate functionalization routes may be investigated. The formation of PE fibres containing 0.1 wt.% Bu-BNNT has demonstrated significantly enhanced ductility and tensile toughness under axial strain whilst maintaining the stiffness and strength of pristine PE. The implications for such nanocomposite fibres are considered in the context of enhanced mechanical properties and also in the context of the impact of embedded nanosheets for enhanced barrier and protection against free radical degradation mechanisms and neutron shielding applications for woven BN:PE textiles.

In summary, exfoliated BNNSs have been covalently functionalized using DBC radicals by the formation of a BCN ring structure within the BNNS lattice. This has been accomplished using a modified phase-transfer reaction methodology whereby BNNSs facilitate migration of dibromocarbenes across the phase boundary and in turn act as the target substrate for covalent bonding of the CBr_2 group. Characterization of the DBC-BNNS material was carried out using HR-TEM, AFM, XRD, SEM-EDX, ToF-SIMS, TGA, Raman, XPS, and FTIR, which underpinned the elucidation of the proposed mechanistic pathway. Characterization of the covalent DBC-functionalization using UV-Vis spectroscopy confirmed the modification of the intrinsic optical transitions within the BNNSs. This result has, firstly, confirmed the ability to use carbenes as a means to surface functionalize BNNSs and secondly, has indicated the viability for band gap manipulation as a consequence of covalent functionalization. To demonstrate the ability to manipulate the surface functionalization of the BNNSs, DBC groups were derivatized to butyl groups by alkyl-halogen exchange and the butyl-functionalized BNNS (BU-BNNSs) used to form PE nanocomposite fibres. Using micromechanical tensile analysis, Bu-BNNS:PE nanocomposite fibres were found to exhibit significantly enhanced ductility and tensile toughness over that of pristine PE fibres. The application of chemically derivatized BNNSs to form nanocomposites highlights the ability to dictate the nature of the interface between nanofiller material and matrix to result in step-changes in

material performance. This work provides a rational basis whereby the intrinsic properties of BN based nanomaterials may be manipulated using covalent functionalization and may be chemically tuned towards their intended application areas.

Acknowledgement. TS and JC would like to thank the European Research Council for funding through the grant SEMANTICS.

Supporting Information Available:

EELS spectra for functionalized BNNS control materials (Figure S1) and DBC-BNNSs indicating Br K-edge (Figure S2). XRD spectra of the (002) and (004) peaks for BNNS and DBC-BNNS (Figure S3, S4). DBC-functionalization density schematic (Figure S5). UV-Vis spectra of $\varepsilon^{1/2}/\lambda$ vs $1/\lambda$ plot for h-BN and DBC-BNNS (Figure S6). Cumulative UV-Vis spectra of DBC-BNNSs indicating band edge and transition state absorption edge (Figure S7). Reaction mechanism for DBC-BNNS alkyl-halogen exchange reaction to form Bu-BNNS (Figure S8). Additional tensile curves of PE and Bu-BNNS:PE nanocomposite fibres (Figure S9).

References

1. (a) Novoselov, K. S. *Science* **2004**, *306*, 666. (b) Radisavljevic, B.; Radenovic, A.; Brivio, J.; Giacometti, V.; Kis, A. *Nat. Nanotechnol*. **2011**, *6*, 147. (c) Pacile, D.; Meyer, J. C.; Girit, C. O.; Zettl, A. *Appl. Phys. Lett*. **2008**, *92*, 133107.

2. Coleman, J. N, et. al. *Science* **2011**, *331*, 568.

3. Liu, N.; Luo, F.; Wu, H.; Liu, Y.; Zhang, C.; Chen, J. *Adv. Funct. Mater*. **2008**, *18*, 1518.

4. Wang, L.; Meric, I.; Huang, P. Y.; Gao, Q.; Tran, H.; Taniguchi, T.; Watanabe, K.; Campos, L. M.; Muller, D. A.; Guo, J.; Kim, P.; Hone, J.; Shepard, K. L.; Dean, C. R. *Science* **2013**, *342*, 6158, 614.

5. Huang, X.; Qi, X.; Boey, F.; Zhang, H. *Chem. Soc. Rev*. **2012**, *41*, 666.

6. Georgakilis, V.; Otyepka, M.; Bourlinos, A. B.; Chandra, V.; Kim, N.; Kemp, K. C.; Hobza, P.; Zboril, R.; Kim, K. S. Chem. Rev. **2012**, *112*, 6156.

7. Zhu, Y.; Murali, S.; Cai, W.; Li, X.; Won Suk, J.; Potts, J. R.; Ruoff, R. S. *Adv. Mater*. **2010**, *22*, 3906.

8. (a) Dreyer, D. R.; Park, S.; Bielawski, C. W.; Ruoff, R. S. *Chem. Soc. Rev*., **2010**, *39*, 228. (b) McGrail, B. T.; Rodier, B. J.; Pentzer, E. *Chem. Mater*. **2014**, *26*, 5806.

9. Xue, Y.; Liu, Q.; He, G.; Xu, K.; Jiang, L.; Hu, X.; Hu, J. *Nanoscale Research Letters* **2013**, *8*, 49.

10. Du, M.; Li, X.; Wang, A.; Wu, Y.; Hao, X.; Zhao, M. *Angew. Chem.Int. Ed*. **2014**, *53*, 3645.

11. Pakdel, A.; Bando, Y.; Golberg, D. *ACS Nano*, **2014**, *8*, 10631.

12. Sainsbury, T.; Satti, A.; May, P.; Zhiming, W.; McGovern, I.; Gun'ko, Y. K.; Coleman, J. N. *J. Am. Chem. Soc.* **2012**, *134*, 18758.

13. Pakdel, A.; Bando, Y.; Golberg, D. *Chem. Soc. Rev*. **2014**, *43*, 934.

14. Lin, Y.; Connell, J. W. *Nanoscale*, **2012**, *4*, 6908.

15. Pakdel, A.; Zhi, C.; Bando, Y.; Golberg, D. *Materials Today*, **2012**, *15*, 256.

16. (a) Tsang, S. C.; Chen, Y. K.; Harris, P. J. F.; Green, M. L. H. *Nature* **1994**, *372*, 159. (b) Stankovich, S.; Piner, R. D.; Nguyen, S. T.; Ruoff, R. S. *Carbon*, **2006**, *44*, 3342.

17. (a) Holzinger, M.; Vostrowsky, O.; Hirsch, A.; Hennrich, F.; Kappes, M.; Weiss, R.; Jellen, F. *Angew. Chem. Int. Ed*. **2001**, *40*, 4002. (b) Park, J.; Yan, M. *Acc. Chem. Res*. **2013**, *46*, (1) 181. (c) Hu, H.; Zhao, B.; Hamon, M. A.; Kamaras, K.; Itkis, M.; Haddon, R. C. *J. Am. Chem. Soc*. **2003**, *125*, 14893.

18. (a) Ikuno, T.; Sainsbury, T.; Okawa, D.; Fréchet, J. M. J.; Zettl, A. *Solid State Commun*. **2007**, *142*, 643. (b) Zhi, C. Y.; Bando, Y.; Terao, T.; Tang, C. C.; Kuwahara, H.; Golberg, D. *Chem. Asian. J.* **2009**, *4*, 1536.

19. Sainsbury, T.; Ikuno, T.; Okawa, D.; Frechet, J.; Zettl, A. *J. Phys. Chem. C* **2007**, *111*, 12992.

20. Wei, D.; Liu, Y.; Wang, Y.; Zhang, H.; Huang, L.; Yu, G. *Nano Lett.* **2009**, *9*, 1752.

21. Niyogi, S.; Bekyarova, E.; Itkis, M. E.; Zhang, H.; Shepperd, K.; Hicks, J.; Sprinkle, M.; Berger, C.; Lau, C. N.; de Heer, W. A.; Conrad, E. H.; Haddon, R. C. *Nano Lett.* **2010**, *10*, 4061.

22. Bhattacharya, A.; Bhattacharya, S.; Das, G. P. arXiv preprint arXiv:1101.5245 (**2011**).

23. Zhou, J.; Wang, Q.; Sun, Q.; Jena, P. arXiv preprint arXiv:0910.5287 (**2009**).

24. Zhang, Z.; Cheng Zeng, X.; Guo, W. *J. Am. Chem. Soc*. **2011**, *133*, 14831.

25. Su, M.-D. *J. Phys. Chem. B* **2005**, *109*, 21647.

26. Li, Y.; Zhou, Z.; Zhao, J. *Nanotechnology* **2008**, *19*, 015202.

27. Cao, F.; Ren, W.; Xu, X.; Ji, Y.-M.; Zhao, C. *Phys. Chem. Chem. Phys*. **2009**, *11*, 6256.

28. Kakkar, R.; Sharma, S. *Chemistry Journal* **2011**, *1*, 9.

29. Doering, W. E.; Hoffman, A. K. *J. Am. Chem. Soc.* **1954**, *76*, 6162.

30. Makosza, M.; Wawrzyniewicz, M. *Tet. Lett*. **1969**, *53*, 4659.

31. Kimura, Y.; Isagawa, K.; Otsuji, Y. *Bull. Univ. Osaka Prefecture, Ser. A, Engineering and Natural Sciences.* **1979**, *28* (1), 49.

32. Yu, J.-G.; Huang, K.-L.; Tang, J.-C. *Physica E* **2008**, *41*, 181.

33. Chua, C. K.; Ambrosi, A.; Pumera, M. *Chem. Commun*. **2012**, *48*, 5376.

34. Ci, L.; Song, L.; Jin, C.; Jariwala, D.; Wu, D.; Li, Y.; Srivastava, A.; Wang, Z. F.; Storr, K.; Balicas, L.; Liu,, F.; Ajayan, P. M. *Nature Nanotech*. **2010**, *9*, 430.

35. Huang, Y.; Bando, Y.; Tang, C.; Zhi, C.; Terao, T.; Dierre, B.; Sekiguchi, T.; Golberg, D. *Nanotechnology* **2009**, *20*, 085705.

36. Lee, C. H.; Wang, J.; Kayatsha, V. K.; Huang, J. Y.; Yap, Y. K. *Nanotechnology* **2008**, *19*, 455605.

37. Singhal, S. K.; Srivastava, A. K.; Singh, B. P.; Gupta, A. K. *Ind. J. Eng. & Mater. Sci.* **2008**, *15*, 419.

38. Bigdeloo, J. A.; Hadian, A. M. *Int. J. Recent Trends Eng*. **2009**, *1*, (5) 176.

39. Li, J.; Vaisman, L.; Marom, G.; Kim, J.-K. *Carbon* **2007**, *45*, (4) 744.

40. Zhi, C.; Bando, Y.; Tang, C.; Xie, R.; Sekiguchi, T.; Golberg, D. *J. Am. Chem. Soc*. **2005**, *127*, 15996.

41. Borowiak-Palen, E.; Pichler, T.; Fuentes, G. G.; Bendjemil, B.; Liu, X.; Graff, A.; Behr, G.; Kalenczuk, R. J.; Knupfer, M.; Fink, J. *Chem. Commun*. **2003**, 82.

42. Yang, D.-P.; Li, Y.-A.; Yang, X.-X.; Du, Y.-H.; Ji, X.-R.; Gong, X.-L.; Su, Z.-P.; Zhang, T.-C. *Chin. Phys. Lett.* **2007**, *24*, (4) 1088.

43. Blum, N. A.; Feldman, C.; Satkiewicz, F. G. *Phys. Stat. Sol. (a)* **1977**, *41*, 481.

44. Höhne, R.; Esquinazi, P.; Heera, V.; Weishart, H. *Diam. Relat. Mater* **2007**, *16*, 1589.

45. Socrates, G. *Infrared and Raman Characteristic Group Frequencies: Tables and Charts*.: John Wiley and Sons Inc.: New York, **2004**.

46. Song, L.; Ci, L.; Lu, H.; Sorokin, P. B.; Jin, C.; Ni, J.; Kvashnin, A. G.; Kvashnin, D. G.; Lou, J.; Yakobson, B. I.; Ajayan, P. M. *Nano Lett*. **2010**, *10*, 3209.

47. Gorbachev, R. V.; Riaz, I.; Nair, R. R.; Jalil, R.; Britnell, L.; Belle, B. D.; Hill, E. W, Novoselov, K. S.; Watanabe, K.; Taniguchi, T.; Geim, A. K.; Blake, P. *Small*, **2011**, *7*, 465.

48. Krause, M.; Bedel, L.; Taupeau, A.; Kreissig, U.; Munnik, F.; Abrasonis, G.; Kolitsch, A.; Radnoczi, G.; Czigány, Z.; Vanhulsel, A. *Thin Solid Films* **2009**, *518*, 77.

49. Conde, O.; Silvestre, A. J.; Oliveira, J. C. *Surf. and Coat. Tech*. **2000**, *125*, 141.

50. Ferrari, A. C.; Rodil, S. E.; Robertson, J. *Phys. Rev. B* **2003**, *67*, 155306.

51. Li, Y.-L.; Zuo, P.; Philips, D. L. *Chem. Phys. Lett*. **2002**, *364*, 573.

52. Shi, Y.; Hamsen, C.; Jia, X.; Kim, K. K.; Reina, A.; Hofmann, M.; Hsu, A. L.; Zhang, K.; Li, H.; Juang, Z.-Y.; Dresselhaus, M. S.; Li, L.-J.; Kong, J. *Nano Lett*. **2010**, *10*, 4134.

53. Mannan, M. A.; Nagano, M.; Shigezumi, K.; Kida, T.; Hirao, N.; Baba, Y. *Am. J. Appl. Sci*. **2007**, *5*, (6) 736.

54. (a) Chanunpanich, N.; Ulman, A.; Strzhemechny, Y. M.; Schwarz, S. A.; Janke, A.; Braun, H. G.; Kraztmuller, T. *Langmuir* **1999**, *15*, 2089. (b) Baker, M. V.; Watling, J. D. *Langmuir* **1997**, *13*, 2027.

55. Marvel, C. S.; Hager, F. D.; Coffman, D. D. *J. Am.Chem. Soc*. **1927**, *49*, 2323.

56. Lee, D.; Song, S. H.; Hwang, J.; Jin, S. H.; Park, K. H.; Kim, B. H.; Hong, S. H.; Jeon, S. *Small* **2013**, *9*, 2602.

57. Zhi, C.; Bando, Y.; Tang, C.; Kuwahara, H.; Golberg, D. *Adv.Mater*. **2009**, *21*, 2889.

58. Harrison, C., Weaver, S., Bertelsen, C., Burgett, E., Hertel, N. and Grulke, E. *J. Appl. Polym. Sci.*, **2008**, *109*, 2529.

Table of Contents Graphic:

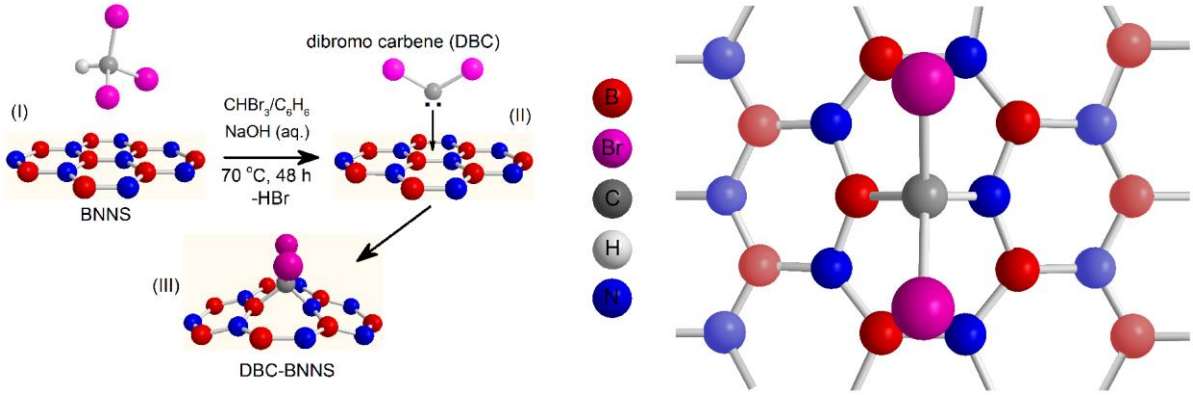

Cover Art Graphic: